

**N90-26455**

**EXPERIMENT K-6-01**

**DISTRIBUTION AND BIOCHEMISTRY OF MINERAL AND MATRIX  
IN THE FEMURS OF RATS**

**Principal Investigator:**

**S. Arnaud  
NASA-Ames Research Center  
SLP 239-17  
Moffett Field, California 94035**

**Co-Investigators:**

**G. Mechanic  
Dental Research Center  
University of North Carolina  
Chapel Hill, North Carolina 27514**

**J. Elliott  
Dept. of Child Dental Health  
London Hospital Medical College  
Turner Street  
London E12AD, England**

**P. Buckendahl  
Thimann Laboratories  
University of California  
Santa Cruz, California 95064**

**E. Katz  
School of Dental Medicine  
University of Connecticut Health Science  
Farmington, Connecticut 06032**

**T. Bromage  
Dept. of Child Dental Health  
The London Hospital Medical College  
Turner Street  
London E12AD, England**

**G. Durnova  
Institute of Biomedical Problems  
Moscow, USSR**

**A. Boyde  
Dept. of Anatomy and Developmental Biology  
University College London  
Gower Street  
London WC1E 6BT, England**

## SUMMARY

Previous analyses of the composition of mineral and matrix in the bone of young rats following space flight has revealed deficits in calcium, phosphorus, and osteocalcin, a non-collagenous protein, without an associated decrease in collagen. To characterize the location and nature of this mineralization defect in a weight bearing long bone, the femur, we attempted to relate the spatial distribution of mineral *in situ* in the proximal, central and distal thirds of the femoral diaphysis to the biochemical composition of bone from the same areas. Biochemical analyses revealed lower concentrations of calcium, phosphorus and osteocalcin but not collagen only in the central third of the diaphysis of the flight animals (F) compared to synchronous controls (S). Collagen concentration was reduced only in the proximal third of the diaphysis, where all 3 crosslinks, expressed as nM/mol collagen, were higher in F than S. A new technique, X-ray microtomography, with a resolution of 26 microns, was used to obtain semi quantitative data on mineral distribution in reconstructed sections of wet whole bone. To improve the resolution of the mineral density distribution, images of the surfaces of cut sections were analyzed by backscattered electrons in a scanning electron microscope (BSE). There was good agreement between the results of the two stereochemical techniques which revealed distinct patterns of mineralization in transverse and longitudinal directions of the diaphysis. The longitudinal gradient in mineral concentrations in the proximal two-thirds of the diaphysis compared well with the semi-quantitative estimates from the microtomography study in F and S. Correlation of mineral concentrations and BSE patterns added a new dimension to our knowledge of the changes in distribution of mineral most vulnerable to the environmental effects in this experiment.

Circulating parameters of skeletal metabolism revealed differences in serum calcium, osteocalcin and alkaline phosphatase, suggestive of steroid hormone excess in the flight animals. These findings, the reduced body weight and enlarged adrenal glands of the flight animals, possibly due to post flight environmental stress, preclude any interpretation of our results with reference to space flight per se. Nevertheless, the novel methodology developed for this flight experiment shows considerable promise in elucidating the biochemical nature of what appear to be regional alterations in the mineralization of long bones of animals exposed to spaceflight.

## INTRODUCTION

Analyses of the morphology (1-4) and biochemical composition (5,6) of the bone of young rats following space flight reveals reduced formation of bone. Quantitatively normal amounts of collagen, reduced content of calcium, phosphorus and a non-collagenous protein associated with hydroxyapatite, indicates that the basic defect is centered in the calcification of collagen.

The collagen fibril, which comprises 90% of the organic matrix of osteoid, is the structural determinant of the mineral content of an element of bone (7,8). The fibril provides microspaces, within its structure, for most of the mineral particles of bone. Events in these spaces serve to orient mineral crystal growth such that the c-axis of a mineral crystal is parallel to the c-axis of the collagen fibril. The lateral dimensions of these mineral particles are constrained by the details of the molecular packing within a fibril.

The findings of an hypomineralized arrest line on the periosteal surface of a tibia (2) and smaller crystallites in density gradients of pulverized bone (9) of young rats in orbit on earlier Soviet and American flights suggest that newly synthesized collagen does not mineralize, and that the maturation of collagen mineralization, initiated on land, is altered in space. This indicates that the fibril structure could be somewhat compressed, perhaps by the same forces which cause the redistribution of extracellular fluids in space flight (10). To determine collagen centered effects in mineralization, it is critical first, to know the mineral concentration and its spatial orientation in hydrated bones. The mechanism of space flight effects on mineralization can then be estimated by

correlating quantitative estimates of mineral density with chemical analyses of mineral and matrix in selected regions, our ultimate goal.

The biochemical analyses of bone carried out in the laboratories of Dr. Mechanic and P. Buckendahl are documented in section I. Technology capable of mapping the distribution of mineral in rat bone to a spatial resolution of about 20 microns and providing reference data in terms of known units, i.e. grams per unit volume, required development and is described in section II by Drs. Bromage, Elliot and Boyde. Section III describes the circulating indices of skeletal metabolism in the four experimental groups of rats and other data essential to the interpretation of structural changes in bone exposed to both post flight environmental changes and space flight.

## I. BIOCHEMICAL ANALYSES OF 3 REGIONS OF THE FEMORAL DIAPHYSIS

This aspect of the study was carried out to determine quantitative estimates of the essential components in bone calcification, collagen and mineral, in the three same regions in which density distribution was analyzed. We have measured the concentration of calcium and phosphorus to relate to the density distribution data. A non-collagenous protein, osteocalcin, associated with hydroxyapatite in mineralized bone was also measured (11). The function of this non-collagenous protein is not known, but its concentration in bone, determined by species specific radioimmunoassay, roughly parallels the mineral content of that bone. Collagen was assayed by the measurement of hydroxyproline, based on a value of 300 residues of hydroxyproline per molecule of collagen. The fibrils of collagen are stabilized by reducible and non-reducible intermolecular crosslinks which may also function to provide the proper distance between collagen molecules in bone for calcification (12). The two principle reducible crosslinks of bone collagen are dihydroxylysinoxoleucine (DHLNL) and hydroxy-lysinoxoleucine (HLNL) (13). A third non-reducible crosslink, pyridinoline, derived from DHLNL crosslinks during the normal process of ageing, is found in high concentration in non-mineralized collagen (14), and may have a role in preventing mineralization. A collagen profile quantitating these 3 crosslinks was also carried out on each third of the femoral diaphysis to relate to the mineral data and stereochemistry.

### Methods and Materials

Our interest in localizing mineralization activity in the diaphysis of the femur to proximal, central and distal thirds made it necessary to pool the bone samples from each experimental group to provide enough material for chemical analysis. The proximal 10 mm of bone with the neck and greater trochanter of the femur and the most distal region of the femur are not included in the powders for chemical analysis. Determinations of collagen and crosslinks were carried out in Dr. Mechanic's laboratory where the bone was pulverized and weighed. Methods are as reported (15,16,17). The mineral and osteocalcin assays were done on a 1 mg aliquot of each pool of powders in P. Buckendahl's laboratory by previously reported methods on an EDTA extract (18). Because statistical analyses of a determination from a single pool could not be done, we selected a value two standard deviations above or below the error of the method to denote the difference in two comparison groups (i.e., exceeding 6 percent for calcium, 12 percent for phosphorus, and 10 percent for hydroxyproline and osteocalcin etc.) See Table I.

### Results

The concentrations of calcium, phosphorus, and osteocalcin are listed on Table II. The differences in the mineral composition are confined to the central section of the diaphyses where concentrations in B and F are the same and lower, by about 50 percent, than either V or S. Figure 1 depicts the percent change in V, S, and F estimated from B for the minerals and osteocalcin. Concentrations in the proximal region of all 3 experimental groups and of the distal region in the vivarium, show little change. The increases in mineral and osteocalcin are in the central or

midshaft in V and S. In F, relative to B, phosphorus and osteocalcin are the same, and calcium 19 percent lower. The concentration of hydroxyproline in F is 14 percent lower than S only in the proximal region.

#### Comment

The data identify two regions in the diaphyses where bone of different chemical composition is generated in the experimental F group, the proximal and central diaphysis.

#### Proximal diaphysis

The chemical composition of the proximal section reveals lower concentrations of collagen and higher concentrations of the reducible crosslinks, DHLNL and HLNL. The increase in crosslink concentration is indicative of new collagen synthesis. The increase in pyridinoline concentration indicates poorly mineralized collagen since pyridinoline formation is reduced when collagen is mineralized. The modest reduction in total collagen reflects accelerated degradation. These results are similar to the results of collagen and crosslink analysis in the femurs of immobilized monkeys (19). See Table III.

#### Central diaphysis

Differences in the mineral concentration were evident only in the central portion of the diaphysis, where values in F were 19 percent lower than the basal controls, and 39 percent lower than S. Given that these measurements represent a single assay of a pool of 4 small sections of the mid-diaphysis, a qualitative interpretation is more appropriate than a quantitative one. We cannot state from the data presented whether the low concentration in mineral is the result of failure of mineral apposition or loss of mineralized bone.

#### Distal diaphysis

The absence of differences in the mineral and osteocalcin composition of the distal section of the femur in B and V and modest increases in both S and F suggests either an influence of diet schedule, caging, or maturity of the animals in the experimental groups for flight, as compared to the vivarium controls. The range of increased concentration of mineral and osteocalcin, unassociated with an increased concentration of hydroxyproline, were the same for all components and ranged from 19 to 25 percent in both F and S. This suggests that these compositional changes were unaffected by either flight or post flight environments.

Clear differences in the biochemistry of distal, central and proximal thirds of the diaphysis of the femur were evident from the above analysis, and require confirmation.

## II. MINERAL DENSITY DISTRIBUTION OF THE FEMORAL DIAPHYSIS

### A. Surface remodeling activity

Illustrated in Figure 2 is the structure and remodeling activity of the surface of the left femur of a 300 gram Czech Wistar rat. The diaphysis of this long bone is the object of this entire study. This specimen in the figure came from an animal used in a pilot study to compare effects of diet and housing at 1 G. This animal was housed in a group cage and received the same diet as the animals in the flight experiment. Scanning electron microscopy (SEM) of the surface of the whole bone was used to identify areas of resorption by the presence of resorption cavities and osteoclasts, and areas of formation by the presence of bundles of collagen associated with active osteoblasts. Active remodeling involves less than one half the periosteal surface, the remainder being in the resting phase. Surface resorption activity is extensive on the distal third, and the neck (proximal),

primarily. Evidence of active formation is confined to two areas on the medial aspect of central and proximal shaft and a third area in the greater trochanter.

The diversity of remodeling activity on the periosteal surface of this bone illustrates the wide range of metabolic activity which occurs simultaneously in a long bone during growth. Our effort is complicated by awareness that surface remodeling does not necessarily parallel the metabolic activities of the interior of the bone at the same levels or the differing rates of acquisition of matrix and mineral in the regions of growing bone. In this study, we used the basal (B) and vivarium (V) controls for estimation of changes during growth.

This surface map and scale is provided primarily for purposes of orientation to our study which details the mineral densities of the proximal, central and distal thirds of the shaft, with analyses beginning 10 mm distal to the proximal tip of the whole bone.

## B. X-ray microtomographic examination of rat femurs

### Methods and Materials

X-ray microtomography is a miniaturized version of the well known X-ray computer tomography (CT scanning) that is used for medical diagnosis. Methods and principals are detailed in the references (20-23). In the microscopic form used in this project, the X-ray beam was 10 microns in diameter and was formed by an aperture in front of a 100 X 100 micron source (silver target, 35 kv, 1.5 ma, 60 microns palladium filter). Sections of the cross-section of the femur are reconstructed from 240 projections, each consisting of 256 points. The X-ray absorption at each point was measured by counting for 5s, so the total observational time for each section was 85.3 hours. The translation of the bone across the X-ray beam was done by mounting it at the end of a pivoted rod which was moved up and down by fixed micrometer. This means that the actual pixel size in the reconstructions is only a nominal 26 microns, and will change slightly when the position of the section along the bone is changed (actually, 28.75 to 26.88 in 5 sections of the synchronous control (S) and 29.10 to 28.63 microns in the 3 sections of the flight femur (F)).

The information that is obtained in the reconstructed section of the bone is the distribution of the linear X-ray absorption coefficient (measured in  $\text{cm}^{-1}$ ) for the particular wavelength of the X-rays used (silver K-alpha) for each of the nominal 26 micron pixels. At this wavelength, by far the biggest contributor to the absorption will be the mineral of bone. This mineral is similar to calcium hydroxy-apatite,  $\text{Ca}_{10}(\text{PO}_4)_6(\text{OH})_2$ , and it makes up about 65 percent of the bone by weight. The linear absorption coefficient of pure hydroxyapatite for silver K-alpha radiation is 15.9  $\text{cm}^{-1}$ . The information for the reconstruction of each section is represented by a 2-dimensional array of numbers, in this case 256 X 256 array in which each number can take one of 256 values. The digital images can be displayed in a number of different forms, including grey scale images of the whole intensity range, expanded grey scale of part of the intensity range and contour maps of constant linear absorption coefficient. Figure 3 illustrates 5 'sections' from S and 3 from F 'cut' at 4 mm intervals starting 10 mm from the tip of the proximal end of the bone at the same intensity and similar grey scales. Two sections are missing from the flight specimen because the distal end of the bone fragmented. Figure 4 illustrates a contour map of the proximal section of S and F femurs drawn at two intensity levels, 150 for interior and 230 for external outlines.

### Results

The quantitative results of the microtomography study are given in Table IV. The control femur shows a decrease in mineralization from the proximal toward the distal metaphysis. The F femur shows a more rapid decrease from the first to the 3rd section, (15 vs 7.5 percent from sections 1 to 3) than S.

## Comment

The results of this study involves a new technique and should be regarded as a first attempt. As far as we know, there is no detailed information about the biological variability of the mineralization along the length of the femur, among different animals of the same or different ages. The clinical characteristics of the two animals whose left femur served as the prototype for this study are given in Table V. As yet no detailed analysis of the digital images is possible because of the need for further work to establish the absorption coefficient values on an absolute scale, to improve the method of tissue preservation, and to repeat these studies in additional specimens. The number of specimens for each of these analyses was the most serious limitation. Chemical analyses could not be done on the same bone subjected to microtomography because of the time required, i.e. more than 80 hours per section.

### C. Image analysis using backscattered electrons in a scanning electron microscope

Previous studies of mass distributions within thin slices of biological tissues have all been made using microradiography. With this technique, it was demonstrated that mineralized bone is not homogenous, and that individual zones of packets have different densities. In lamellar bone, the mineral content is lowest at the time of formation and slowly increases during a maturation process as osteons age. Primary membrane (woven) bone mineralizes rapidly, and to a level which is slightly higher than that of mature lamellar bone. The density of newly formed lamellar bone packets is 70-80% of that achieved in fully mature bone. A computerized system for the analysis of mineral densities from microradiographs has been described but no studies conducted with it have so far been published (24).

The backscattering of electrons is a process which is dependent on the atomic number of an element and hence is also proportional to density. We have previously shown that the mineral density distribution within bone can also be studied using backscattered electron (BSE) imaging in the scanning electron microscope (SEM). BSE images of flat (cut and polished or micromilled) bone surfaces resemble microradiographs: the darker an area appears, the less mineral it contains. However, these images have a much higher spatial resolution than microradiographs because BSE are collected from only a thin layer at the surface of the specimen. Since a surface is examined, they are also not subject to false contrasts due to variations in section thickness.

### Methods and materials

The BSE signal can be thresholded and pixels counted to measure the phase volumes of bone lying within given density fractions (25,26). We have used this approach to study the density distributions in femur samples from the Cosmos 1887 experiment. The amount of bone having discrete, constant density ranges was measured using an image analysis system interfaced directly to the SEM (27).

The specimens were 150  $\mu\text{m}$  thick transverse sections cut from the proximal, central and distal thirds of the femurs from each experimental group. The thick sections were embedded in methyl methacrylate, copolymerised with styrene to enhance the stability of the resin under electron bombardment. After hardening was complete, topography-free surfaces were prepared by careful grinding and polishing and the specimens rendered electrically conductive by sputter coating with a layer of silver.

The image analysis system was interfaced directly to the SEM. The BSE signal was digitized at each pixel during a single slow scan of the electron beam across the sample and converted to grey level histograms. The pixel data was allocated to one of eight equal-width grey level bins in RAM which spanned the range from peak black to peak white (i.e., 0-5 volts) in the BSE image. Non-bone, marrow spaces, vascular canals and osteoid were all assigned bin "zero", least dense to 1 and

most dense mineral to bin 7. The percentage area of each density level was printed after each scan and is expressed as the percentage of the total of mineralized tissue analyzed.

We selected operating conditions as a working compromise between pixel resolution and sampling density. Effective pixel size was roughly 0.2 $\mu$ m diameter and we could resolve useful detail at 500X in a 100 mm diameter, 1000 line image. Pixels were widely spaced at the specimen, constituting a "stereological grid" sampling the surface composition at intervals. Four fields were analyzed per specimen, centered on the medial lateral, anterior and posterior cortices. We used System 80K software (Sharp MZ 80K microcomputer) interfaced to a Cambridge Stereoscan S4-10 SEM, operated at an accelerating voltage of 19.3kV. To ensure the same operating conditions for the specimens, a special carousel stage was developed for continuous analysis of specimens arranged to alternate experimental groups and levels. Drift was checked by returning to the starting field of the first specimen of the run. We were able to reproduce the image analysis data on successive runs of the same samples, but there are problems in setting up identical operating conditions on repeated occasions. Although we have attempted to set up the system against known, pure standards (e.g. polished aluminium and fluoroapatite), we have not yet found uniform, characterized materials which fall at the margins of the range of densities we wish to cover.

## Results

### 1. The amount unmineralized tissue per field analyzed (Bin zero)

The value in the first bin of each histogram fluctuates mainly as a consequence of variations in the thickness of the cortex. The lowest value recorded (at 23%) reflects the largest amount of mineralized bone present in the field of view, i.e. the "solid bone" contains 23% of osteocyte lacunae plus blood vessel canals, plus non-mineralized osteoid. The highest values (at about 75%) reflect very thin bone which did not fill the 1mm wide field of view. The amount of non mineralized tissue analyzed for each experimental group was nearly identical: for B, V, S, and F, values were 59, 55, 56, and 57% in bin 0, respectively.

### 2. Modal density as a function of experimental group

Average mineralized tissue analyzed was 42.25%. A histogram of the percent calcified tissue in each bin for each experimental group is illustrated in Figure 5 which shows the modal density in each bin, according to Table VI.

The density distribution of the entire diaphysis of the flight bone resembles that in the preflight B more than either of the age matched controls. The density spectrum of each group cannot be considered to be different from any other group, however, because of the large variation in the bones of each group (n=5 in B and V, 4 in S and F).

### 3. Modal density as a function of longitudinal position

There appears to be one type of pattern for the pair of B and V, and a second type for the pair S and F. To compare S and F, we have separated the pairs in Table VII which enumerates the percent mineral in bins < 3 and > 6 in the proximal, central and distal regions.

Low density fractions are most abundant in the distal regions of the femoral shaft, as expected in growing animals. The variation in the central segment is striking, and may reflect either biological diversity or a problem with technique or both. In this central segment, the highest percentage of dense fractions are found, as might be expected in the midshaft of cortical bone.

Variation in the proximal segment in each experimental group is also apparent. The F group has half as much low dense bone as its pair, S. Percentages in bin 0 for F and S were the same, 55% and 53%. Feeding schedules and housing are the same in B and V, but differ from S and F, a possible explanation for the different longitudinal distribution of mineral during growth.

#### 4. Histograms as a function of anatomical quadrant

Averaged results for all experimental groups and for the 3 longitudinal positions are similar with the grand mean showing the predominant density levels in the central bins, 3, 4, and 5, as follows: 6/13/20/20/19/14/5 for bins 1-7, respectively. Of interest are the higher values for the most dense bin in 3 quadrants (not lateral) of the midshaft and for the least dense bin in the distal shaft in F than S. These apparent regional density differences may account for the flatter appearance of the histogram of the whole diaphysis in figure 5 (central F, 0/0/1/8/27/36/24 and central S, 0/1/2/10/39/40/5; distal F, 23/36/28/3/0/0/0 and distal S, 6/24/44/19/2/0/0). The histograms in figure 6 show the density profile of the lateral quadrant (selected for graphic presentation because of low intra-group variation) of the 3 longitudinal sections in S and F.

#### Comment

The technique of BSE and SEM appears to be a powerful method to identify regional differences in mineral density distribution capable of determining the effects of space flight on calcification. However, we can draw no conclusions from any of the data acquired at this time for a number of reasons. Major problems which introduce uncertainty in the data are the fractures, possibly due to rapid freezing. Group comparisons pose problems of matching levels in bones of slightly different size in growing animals of different age. Apparent differences observed may be related to artifacts of sample preservation and other aspects of the newly developed techniques. The number of bones examined was too small to establish statistical validity of any of the observations in the regions and there is considerable variation in mineral density distribution of the specimens in each group. There is as yet no data base established for reference of space flight data to changes with age, diet, and other variables known to affect mineral density.

On the other hand, we regard this as a first successful attempt to document regional mineral gradient densities in the femoral diaphysis of the rat. The density levels in the longitudinal direction are consistent with our understanding of normal physiology, with least dense fractions predominating in the distal region and intermediate density fractions predominating in the central region of cortical bone. The dissimilarity in the high density fraction percentages in the pairs B/V and S/F may be related to different growth activities of these pairs from different habitats. Also, there are similarities in these results to those derived from density gradients of powdered cortical bone from the femur of rats 7 days in space. Simmons et al observed a trend for density profiles to shift toward the higher density fractions post flight (9). The unique and novel aspects of this study are observations of apparent regional differences in the patterns of mineral density distribution in both horizontal and longitudinal directions which we hope to confirm in experiments in future space flights.

#### CORRELATION OF BIOCHEMISTRY WITH IMAGE ANALYSIS

To attempt to relate the measured elements in bone to density images is a challenge because the distribution density is referenced to 100 percent of an area, and the chemical measures are referenced to a known mass, i.e. microgram, which may be distributed sparsely (low density) or in a more compact way (high density) in the same area. In spite of this we tried to relate these sets of data, by comparing the fraction or percent of mineral or unmineralized collagen of the chemical assays to the percent of high, low or soft tissue density in the 3 sections of diaphysis in F and S.

The proximal region shows half as much mineral in F in the low density bins (31 vs 63) and a smaller increment in the higher density bins than in S (6 vs 0 percent) with no change in the concentration of mineral or collagen. This could indicate less newly mineralized collagen in F, consistent with the crosslink concentrations. Only the lateral quadrant shows an increase in uncalcified tissue (see Figure 6) in bin 0. The sum of all quadrants for bin 0 is 55 for F and 53 for S, consistent with morphologic data which fails to show increases in unmineralized osteoid in cross sections of long bones after space flight.

The central region shows the scant amount of mineral in F to be more distributed in the high density fractions compared to S. There is only 2 percent less in the low density fractions of F vs S.

The distal regions show 15 percent less mineral in the low density fractions in F compared to S.

The above suggests shows regional variation in the concentration and distribution of matrix and mineral which is consistent, and similar to the findings of Rogacheva et al after a longer flight (3). Of interest is the low concentration of mineral in the mid section where measurements of reduced breaking strength are reported (28,29).

### III. CIRCULATING INDICES OF SKELETAL METABOLISM AND OTHER CLINICAL CHARACTERISTICS OF ANIMALS RATS IN COSMOS 1887 FLIGHT

Essential to the interpretation of structural changes in bone exposed to microgravity is an evaluation of the animals calcium metabolism, bone cell activity, nutritional and endocrine status at the time of the necropsy. For this purpose, the small amount of serum available for study was analyzed for a few constituents that have relevance to the bone biochemistry study.

Total serum calcium and total protein can be a reflection of hydration. Osteocalcin in serum, originates from the osteoblast and has been shown to correlate well with indices of bone formation (30). Another product of the osteoblast in blood, alkaline phosphatase, may also originate in the liver. The enzyme originating in bone is heat sensitive and can be distinguished from hepatic enzyme partly by an assay for the heat sensitive component which we used in this study (31). Serum 25-hydroxyvitamin D is the best indicator of the status of vitamin D nutrition (32), always a consideration when evaluating mineralization since low levels are associated with vitamin D deficiency bone disease. Serum levels of corticosterone were assayed to determine relationships between circulating levels of osteocalcin, known to be depressed by this steroid (33).

#### Results

The results are enumerated on Table VIII. Flight animals showed lower body weight, serum total calcium, and osteocalcin than S. Serum alkaline phosphatase, and adrenal weights were higher in F than in S.

#### Comment

The clinical data in this experiment indicate that there were two factors in addition to space flight which may have contributed to the the mineralization defects. The low body weights of F, the same as the preflight group, are indicative of either failure to gain or of weight loss during their stay in the Siberian forest. If they did not eat for two days before necropsy, the absence of a dietary source of calcium may have stimulated bone resorption. The large adrenal glands of the flight animals suggest high levels of endogenous steroids which we could not demonstrate because of the large range of variation in all groups. Excess adrenal steroids regularly cause metabolic bone disease manifested by increased bone resorption and reduced bone formation. As well, high steroid levels may be directly responsible for suppressing the formation of osteocalcin, reduced to a greater degree in this flight than the 7 day Spacelab 3 flight (55 vs 22%) (5). Of interest is the

relationship between the adrenal gland weights and the circulating level of osteocalcin as shown in Figure 7. The flight group is clearly separated from the controls, an indication of the impact of excess steroid on the activity of the osteoblast, and possibly on the changes we observed.

## REFERENCES

1. Morey ER and Baylink DJ. Inhibition of bone formation during spaceflight. 201:1138-1141, 1978.
2. Turner RT, Bell NH, Duval P, Bobyn JD, Spector M, Holton EM, and Baylink DJ. Spaceflight results in formation of defective bone. Proc Soc Exptl Biol Med 174:224-228, 1983.
3. Rogacheva IV, Stupakov GP, Volozhin AI, Pavlova MN, and Polyakov AN. Rat bone tissue after flight aboard COSMOS-1129 Biosatellite. Moscow Kosmicheskaya Biologiya I Aviakosmicheskaya Meditsina 18:39-44, 1984.
4. Yagodovskiy US, Trifanidi LA, Goroklova GP. Space flight effects on skeletal bones of rats: light and electron microscopic examination. Aviat Space and Environ Med. 47:734-740, 1976.
5. Patterson-Buckendahl P, Arnaud SB, Mechanic GL, Martin RB, Grindeland RE, and Cann CE. Fragility and composition of growing rat bone after one week in spaceflight. Am. J. Physiol. 252:R240- R246, 1987.
6. Prokhonchukov AA, Desyatnichenko KS, and Tigranyan RA. Mineral phase and protein matrix of rat osseous tissue following flight aboard the Cosmos-1129 biosatellite. Space Biol and Med 16:87-92, 1982.
7. Glimcher MJ. Molecular Biology of Mineralized Tissues with Particular reference to Bone. Rev Modern Physics 31:359-393, 1956.
8. Katz EP and Li ST. The Structure and Function of Bone Collagen. J Mol Biol 80:1-15, 1973.
9. Simmons DJ, Russell JE, and Grynblas MD. Bone maturation and quality of bone material in rats flown on the space shuttle 'Spacelab-3 Mission'. Bone and Mineral 1:485-493, 1986.
10. Linnarson D, Tegner B and Eiken D. Effects of gravity on the fluid balance and distribution in man. Physiologist 28:S28-29, 1988.
11. Price PA, Otsuka AS, Poser JW, Kristaponis J and Raman N. Characterization of a gamma-carboxyglutamic acid-containing protein from bone. Proc Natl Acad Sci. USA 73:1447-1451, 1976.
12. Mechanic GL, Banes AJ, Henmi M, and Matsuo Y. Possible collagen structural control of mineralization In The Chemistry and Biology of Mineralized Tissues, Butler WT, Ed. Ebsco Media, Birmingham. pp 98-102, 1985.
13. Mechanic GL, Gallop PM, Tanzer ML. The nature of crosslinking in collagens from mineralized tissues. Biochem & Biophys Res Comm 45:644-653, 1971.
14. Banes AJ, Yamauchi M, and Mechanic GL. Non-mineralized and mineralized compartments of bone: the role of pyridinoline in nonmineralized collagen. Biochem & Biophys Res Comm. 113:975-981, 1983.



15. Yamauchi M, London RE, Guenat C, Hashimoto F, and Mechanic GL. Structure and formation of a stable histidine-based trifunctional cross-link in skin collagen. *J Biol Chem* 262:11428-11434, 1987.
16. Yamauchi M, Katz EP, and Mechanic GL. Intermolecular cross-linking and stereospecific molecular packing in type I collagen fibrils of the periodontal ligament. *Biochemistry* 25:4907-4913, 1986.
17. Mechanic GL, Katz EP, Henmi, Noyes C, and Yamauchi M. Locus of a histidine-based stable trifunctional, helix to helix collagen cross-link: stereospecific collagen structure of type I Skin Fibrils. *Biochemistry* 26:3500-3509, 1987.
18. Patterson-Allen PE, Brautigam CE, Grindeland RE, Asling CW, and Callahan PX. A specific radioimmunoassay for osteocalcin with advantageous species cross reactivity. *Anal Biochem* 120:120:1-7, 1982.
19. Mechanic GL. Personal communication.
20. Elliott JC and Dover SD. Three dimensional distribution of mineral in bone at a resolution of 15 microns determined by X-ray microtomography. *Metabolic Bone Dis and Rel Res* 5:219-221, 1984.
21. Elliott JC and Dover SD. X-ray microscopy using computerised axial tomography. *J. Microscopy* 138:329-331, 1985.
22. Bowen DK, Elliott JC, Stock SR and Dover SD. X-ray microtomography with synchrotron radiation. *SPIE X-ray Imaging II*, 691:94-98, 1986.
23. Elliott JC, Bowen DK, Dover SD, and Davies ST. X-ray tomography of biological tissues using laboratory and synchrotron sources. *Biological Trace Element Res.* 13:219-227, 1987.
24. Phillips HB, Owen-James S, Chandler B. Quantitative Histology of Bone: A computerized method of measuring the total mineral content of bone. *Calc Tiss Res* 26:85-89, 1978.
25. Boyde A. New methods for SEM bone stereology. *Calc Tiss Int* 33:Suppl, abst 43, 1981.
26. Boyde A, Reid SA, Howell PGT. Stereology of bone using both backscattered electron and cathodoluminescence imaging for the SEM. *Beitr Elektronenmikroskop Direktabb Oberfl (Muenster)* 16:419- 430, 1983.
27. Howell PGT, Reid SA. A microcomputer-based system for rapid on-line stereological analysis in SEM. *Scanning* 8:129-144, 1986.
28. Spengler DM, Morey ER, Carter DR, Turner RT, and Baylink DJ. Effects of spaceflight on structural and material strength of growing one. *Proc Soc Exptl Biol Med* 174:224-228, 1983.
29. Dobelis MA, Saulgozis Yu. Zh., Novikov VY, Ilin YA, and Oganov VS. Effect of weightlessness and some of its models on mechanical properties of animal bones submitted to torsion. *Moscow Kosmicheskaya Biologiya I Aviakosmecheskaya Meditsina* 19:40-45, 1985.
30. Price PA, Parthemore JG, and Deftos LJ. A new biochemical marker for bone metabolism. *J. Clin Invest.* 66:878-883, 1980.

31. Posen S, Neal FC, Club JS. Heat inactivation in the study of human alkaline phosphatase. *Ann Int Med* 62:1234-1243, 1965.

32. Arnaud SB and Meger J. A micro-assay for 25-hydroxyvitamin D: method and interpretation *In ASBMR Workshop on Calcitropic Hormone Measurements*, Ed D. Bikle, Springer-Verlag, 1983, Chapter 5.

33. Patterson-Buckendahl PE, Grindeland RF, Shakes DC, Morey-Holton ER, Cann CE. Circulating osteocalcin is inversely responsive to changes in corticosterone. *Am J Physiol* 254:R828-833, 1988.

TABLE I. The weight of the bone powders, in milligrams, from each section of the diaphysis were comparable in each experimental group:

Group	Proximal	Central	Distal	Total/bone
B	104.6	74.2	197.4	376
V	109.6	79.2	196.2	385
S	123.5	86.5	233.5	444
F	109.8	83.8	211.5	405

TABLE II. Concentration,  $\mu\text{g}/\text{mg}$ , in 3 regions of femoral diaphysis.

	B	V	S	F
<b>Calcium</b>				
Proximal	171	150	179	173
Central	93	139	123	75 *
Distal	167	170	215	206
<b>Phosphorus</b>				
Proximal	89	77	95	89
Central	45	71	65	42 *
Distal	86	88	102	104
<b>Osteocalcin</b>				
Proximal	2.20	2.00	2.22	2.10
Central	0.88	1.79	1.48	0.77 *
Distal	1.74	1.82	2.18	2.15
<b>Hydroxyproline</b>				
Proximal	---	---	31.0	26.6 *
Central	---	---	22.2	22.2
Distal	---	---	28.8	28.8

\*indicates a value outside error of method in F relative to S

TABLE III. Concentration of Crosslinks, nM/mol Collagen

Crosslink	S	F
<b>Dihydroxylysinoxidoreucine</b>		
Proximal	0.47	1.70 *
Central	0.81	0.75
Distal	0.77	0.66
<b>Hydroxylysinoxidoreucine</b>		
Proximal	0.13	0.46 *
Central	0.28	0.28
Distal	0.30	0.28
<b>Pyridinoline</b>		
Proximal	0.12	0.34 *
Central	0.15	0.13
Distal	0.24	0.28

TABLE IV: Maximum values of the linear absorption coefficient  $\text{cm}^{-1}$  from the control and flight femur microtomography study

Section #	S	F
1	7.20	7.63
2	6.86	7.23
3	6.76	6.46
4	6.65	
5	6.51	

TABLE V: Body and adrenal weight, serum corticosterone and indices of skeletal metabolism in two rats whose femurs were analyzed by X-ray microtomography.

	Synchronous Control #6	Flight #6	Vivarium range
Body weight, gms	345	304	295 - 345
Adrenal, mg/100 gm body weight	11.3	15.8	11 - 13
Serum total calcium, mg/dl	10.4	8.8	9.6 - 11.4
Total protein, g/dl	6.8	6.8	6.1 - 7.3
Alkaline phosphatase, IU/L	50	112	35 - 67
Osteocalcin, ng/ml	154	60	130 - 166
25-hydroxyvitamin D, ng/ml	18	19	18 - 20
Corticosterone, ug/dl	12.2	8.6	1.8 - 17.8

TABLE VI: Average modal densities or gray levels for whole diaphysis

Experimental group	#1	#2	#3	#4	#5	#6	#7
Basal	9	15	15	15	20	16	5
Vivarium	2	7	19	27	23	13	4
Synchronous Control	4	15	27	20	15	13	2
Flight	9	14	17	16	17	14	8

TABLE VII. Percent mineral in bins of low and high density

	B	V	B	V	S	F	S	F
	<3		>6		<3		>6	
Proximal	11	5	24	45	63	31	0	6
Central	12	19	41	4	3	1	45	60
Distal	79	94	0	0	87	74	0	0

TABLE VIII. Body and adrenal weights, circulating parameters of skeletal metabolism in the rats flown on the Cosmos 1887 biosatellite mission. (Mean  $\pm$  SD)

	Basal	Vivarium	Synchronous	Flight
Body weight, g	316 $\pm$ 19	342 $\pm$ 17	349 $\pm$ 13	303 $\pm$ 5 *
Adrenal weight, mg/100g BW	13.5 $\pm$ .5	12.5 $\pm$ .9	12.5 $\pm$ .8	16.8 $\pm$ 1.5 *
Serum total calcium, mg/dl	10.7 $\pm$ .6	10.5 $\pm$ .7	10.1 $\pm$ .3	9.5 $\pm$ .6*
Total proteins, g/dl	6.5 $\pm$ .2	6.8 $\pm$ .2 +	6.8 $\pm$ .6	6.6 $\pm$ .6
Osteocalcin, ng/ml	227 $\pm$ 20	148 $\pm$ 16#	166 $\pm$ 22	74 $\pm$ 12 *
Alkaline phosphatase, IU/L	97.4 $\pm$ 21	53.8 $\pm$ 12	46.4 $\pm$ 9	70 $\pm$ 29
25-hydroxyvitamin D, ng/ml	20 $\pm$ 5	19 $\pm$ 1	20 $\pm$ 2	20 $\pm$ 1
Corticosterone, ug/dl	11.7 $\pm$ 5	10.1 $\pm$ 6	10.5 $\pm$ 6	15.6 $\pm$ 9

\* p<.05 compared to Synchronous, # p<.05 compared to basal, +n=3

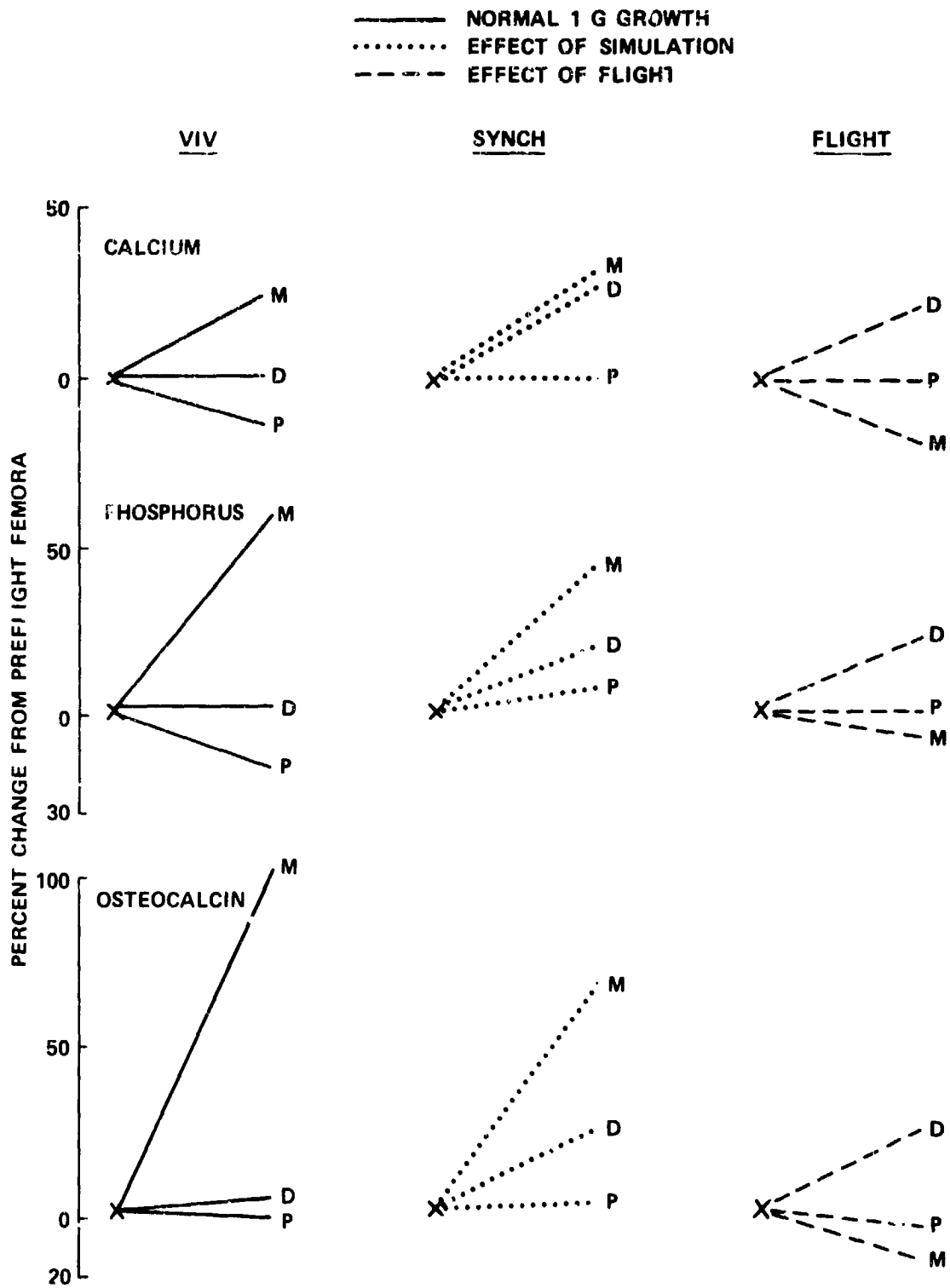


Figure 1. The percent change in the average concentration of calcium, phosphorus, and osteocalcin in the vivarium, synchronous control and flight groups in the proximal (P), central (C), and distal (D) thirds of the diaphysis of the femur, referenced to the basal control for all groups. Concentration of mineral shows increases expected with age in V and S in the mid-diaphyseal region, but not in the flight group.

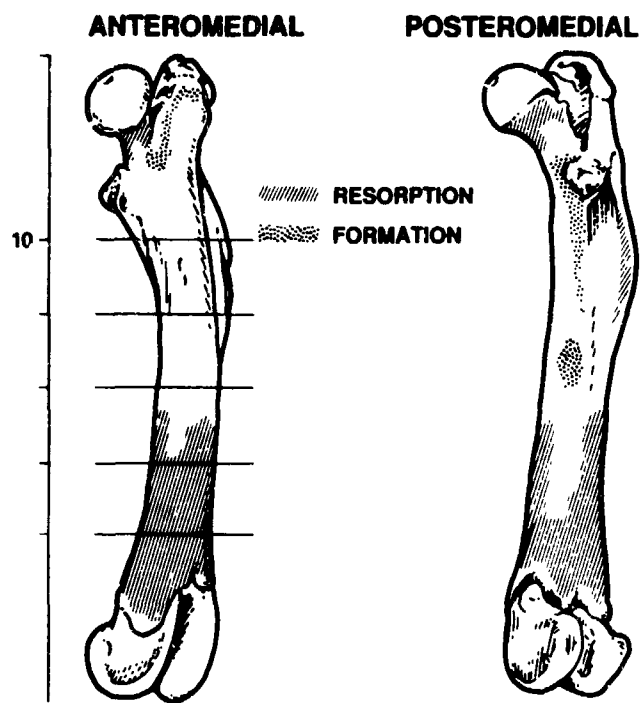


Figure 2. Line drawings from a photograph of the femur of a 300 gram Wistar Czech rat. Surface areas of resorption and formation determined by scanning electron microscopy are depicted. Areas of resorption were identified by resorption cavities and osteoclasts, and of formation by collagen bundles and active osteoblasts.

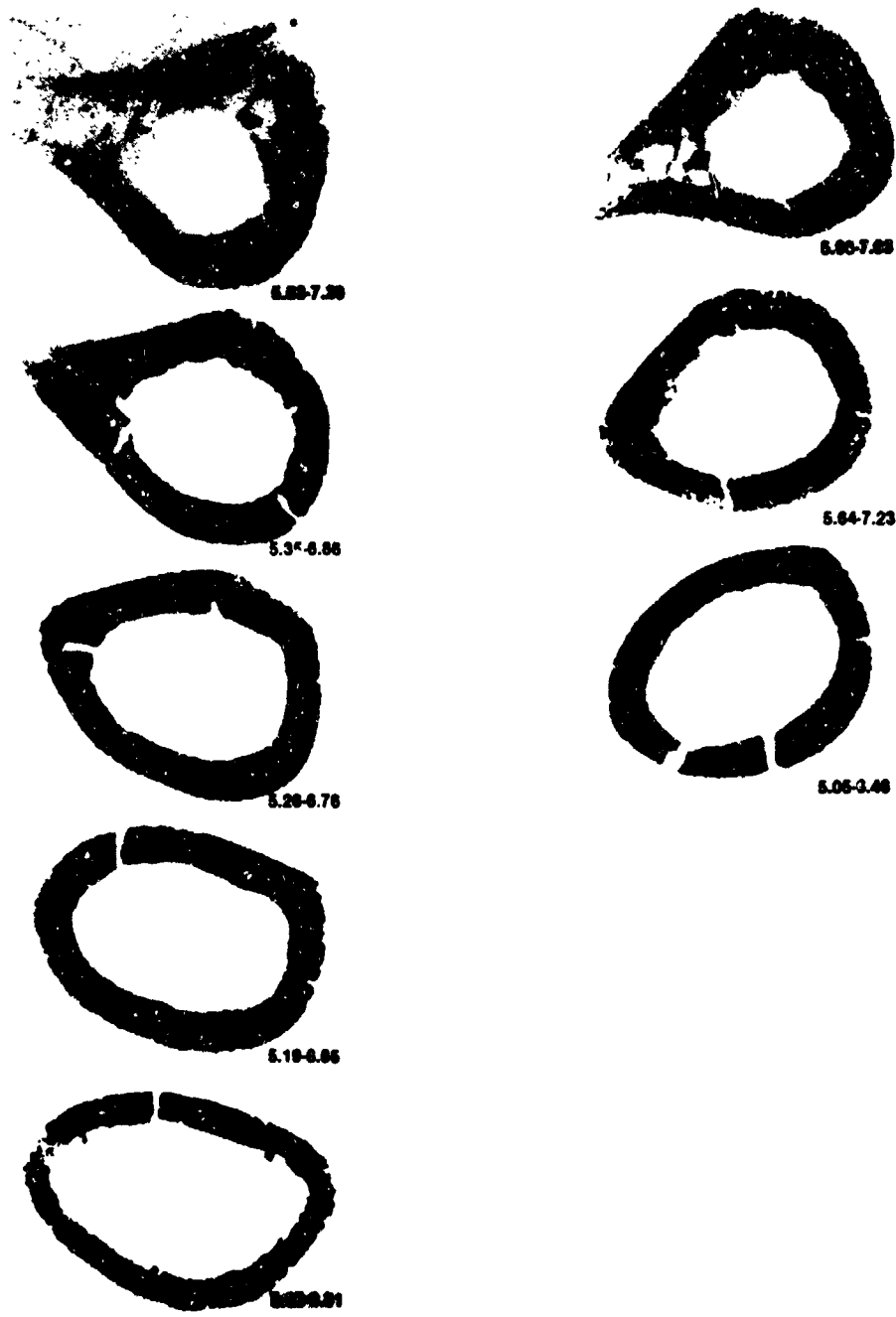
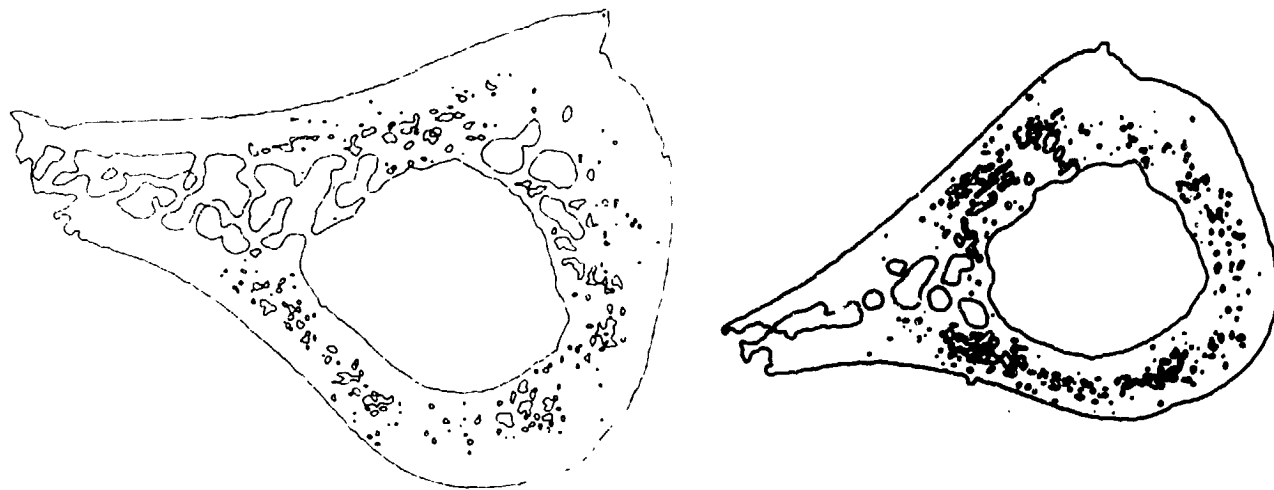


Figure 3. X-ray microtomography of 5 computer generated sections of a synchronous control femur, 4 mm apart, beginning 10 mm from the top of the bone on the left. Three 'sections' from the same locations in the diaphysis of a flight animal. See text for details of the method. Intensity range 200-250, resolution 26-28 microns.





(a) SYNCHRONOUS CONTROL

(b) FLIGHT FEMUR

Figure 4. Contour map drawn from x-ray microtomography sections at two levels of intensity, 150 for interior and 230 for exterior lines.

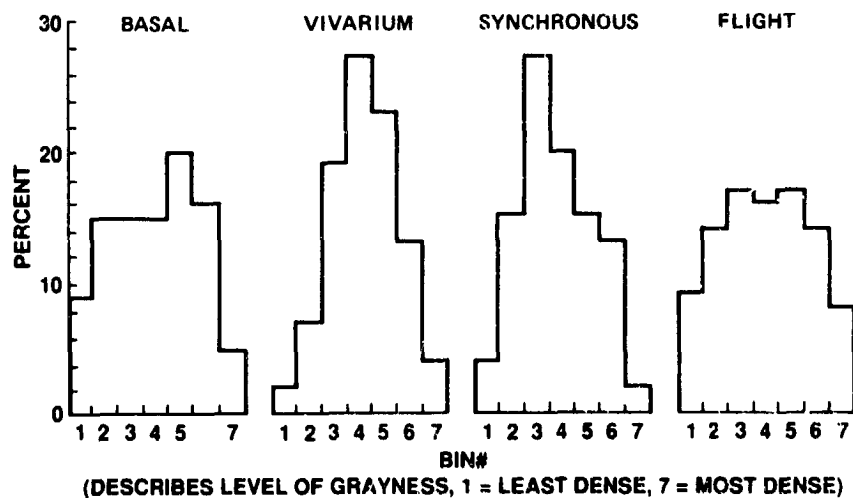


Figure 5. Histograms of the modal densities of combined proximal, central, and distal sections of the diaphysis in 4 experimental groups obtained by backscattered electrons and an image analysis system interfaced directly to a scanning electron microscope. The columns, 1-7, represent the percent of the mineralized bone fraction falling within a fixed computer-selected density range from 1 (least dense) to 7 (most dense).

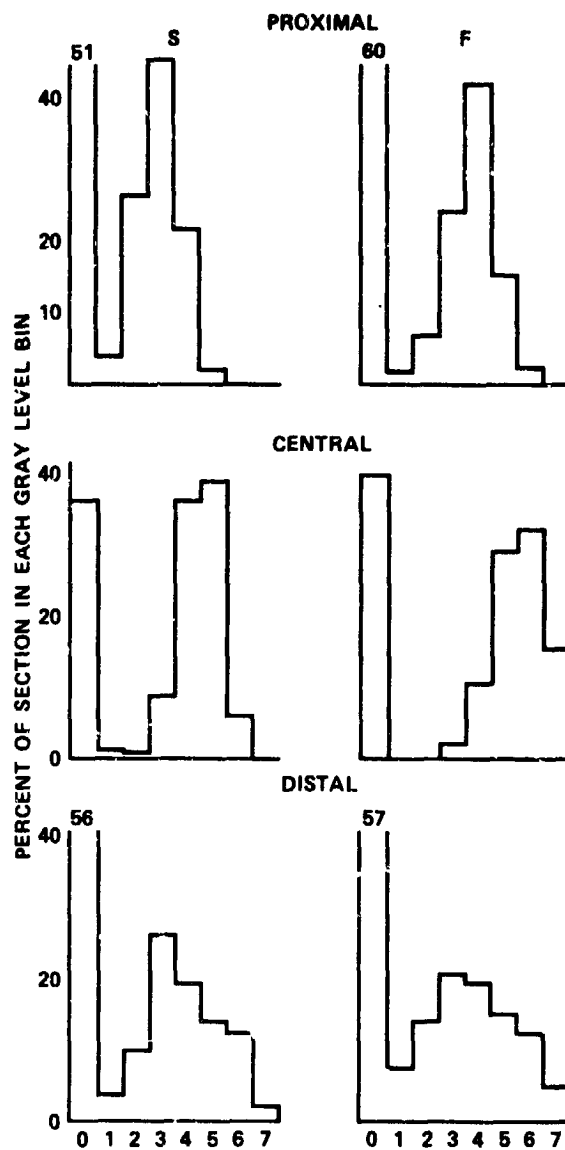


Figure 6. Histograms of the modal densities of the lateral quadrants of proximal, central, and distal sections of the femoral diaphyses of synchronous control and flight groups. Bar heights are the averages of data from 4 animals in the proximal and distal regions, and of 3 in the central region. Note bin 0 (non-bone and osteiod) in the proximal and bins 3 and 7 of the central regions of the flight group compared to the control.

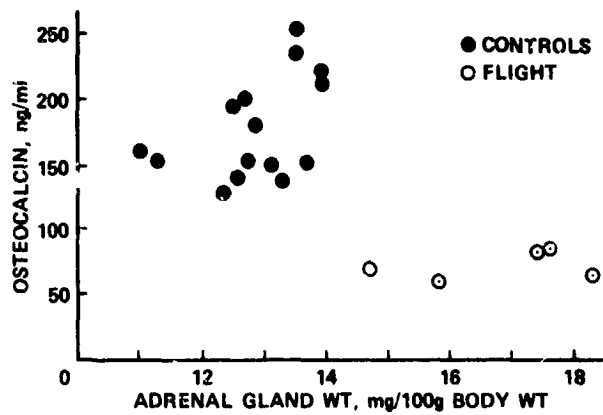


Figure 7. The concentration of serum osteocalcin, ng/ml, as a function of the weight of the adrenal gland, mg/100 g body weight, of flight and all controls.